INTERNATIONAL JOURNAL OF ENVIRONMENT, ENGINEERING & EDUCATION

ISSN 2656-8039 (ONLINE)
VOLUME 8 • ISSUE 2 • JUNE 2026

Received: 2 May 2026 | Accepted: 29 May 2026 | Published: 4 June 2026

Research Article

Map-Derived Agreement Assessment of Landsat-9 OLI-2 for Island-Scale Lithological Discrimination in a Humid Tropical Setting from Langkawi Island, Malaysia

Yaokai Du [a] • Ying Jia Teoh [a,*] • Nur Azwin Ismail [a] • Ismail Ahmad Abir [a] • Haylay Tsegab Gebretsadik [b]

[a] School of Physics, Universiti Sains Malaysia, Penang, Malaysia | [b] Department of Geoscience, Universiti Teknologi PETRONAS, Perak, Malaysia

ABSTRACT

Lithological discrimination in humid tropical islands remains constrained by dense vegetation, deep weathering, regolith cover, mixed pixels, and discontinuous bedrock exposure, which collectively weaken diagnostic spectral responses. This study evaluates the capability and limitations of Landsat-9 OLI-2 for island-scale lithological discrimination in Langkawi Island, Malaysia, using an interpretable optical-only workflow. Atmospherically corrected Landsat-9 imagery was processed through false-color composites, Optimum Index Factor (OIF)-based band selection, band-ratio enhancement, Principal Component Analysis (PCA), Normalized Difference Vegetation Index (NDVI), Jeffries–Matusita separability analysis, and Maximum Likelihood Classification (MLC). The resulting MLC lithological map was assessed pixel-by-pixel against a published geological map; consequently, the reported statistics represent map-derived agreement rather than independent field-validated lithological accuracy. Results show that the OIF-selected RGB 6-5-2 composite, selected band-ratio combinations, and PCA enhanced broad contrasts among Quaternary Alluvium, granitic terrain, and carbonate-bearing formations. The MLC classification achieved an overall map-derived agreement of 51.72% and a kappa coefficient of 0.4177. Qal, Cm-SS/Sh/Md, and OS-Ls/SS showed relatively stronger agreement, whereas PT-Ls/Mb, DP-St/Md, and Tr-Gr were more affected by spectral overlap and class confusion. NDVI-stratified assessment further confirmed that vegetation cover influences classification performance, with low-vegetation areas producing higher agreement than moderate-vegetation areas. This study establishes a reproducible full-island baseline for evaluating optical multispectral lithological mapping under humid tropical conditions. These findings demonstrate that Landsat-9 OLI-2 can support reconnaissance-level lithological discrimination in humid tropical islands but remains insufficient for precise formation-level mapping without field validation and integration with SAR, DEM-derived, or higher-resolution spectral datasets.

KEYWORDS earth observation • geological remote sensing • geospatial monitoring • multispectral classification • multispectral image analysis • sustainable land management • vegetation masking

ARTICLE CITATION

Y. Du, Ying J. Teoh, Nur A. Ismail, Ismail A. Abir, Haylay T. Gebretsadik, "Map-Derived Agreement Assessment of Landsat-9 OLI-2 for Island-Scale Lithological Discrimination in a Humid Tropical Setting from Langkawi Island, Malaysia," International Journal of Environment, Engineering and Education, Vol. 8, No. 2, pp. 264-281, 2026. https://doi.org/10.55151/ijeedu.v8i2.512

***CORRESPONDENCE**

Ying Jia Teoh tyj@usm.my School of Physics, Universiti Sains Malaysia, 11800 USM, Penang, Malaysia https://orcid.org/0000-0003-0519-5188

1. INTRODUCTION

Lithological mapping in humid tropical regions remains a persistent challenge in geological remote sensing because dense vegetation, deep weathering profiles, heterogeneous regolith, soil moisture, and discontinuous rock exposure often obscure the diagnostic spectral response of bedrock. In such environments, satellite sensors rarely record the spectral signal of fresh lithology alone; instead, the recorded reflectance commonly represents mixed responses from vegetation, weathered materials, surficial deposits, anthropogenic surfaces, and exposed rock fragments. This problem is particularly acute on tropical islands, where rugged topography, coastal sediments, karstic terrains, granitic bodies, clastic successions, and alluvial deposits occur within relatively small spatial domains. Consequently, lithological boundaries in satellite imagery are frequently transitional, spectrally mixed, and difficult to separate using optical data alone. Despite these limitations, remote sensing remains indispensable for regional geological mapping, especially in areas where field access is constrained by vegetation density, terrain complexity, cost, and logistical limitations [1]–[4].

Among available Earth observation datasets, Landsat imagery continues to play an important role in geological and lithological applications because of its long-term data continuity, global coverage, open accessibility, and moderate spatial and spectral resolutions, which are suitable for regional-scale mapping. Landsat-9 OLI-2 provides multispectral information in the visible, near-infrared, and shortwave-infrared regions, which are relevant for detecting broad differences in iron-bearing minerals, clay-rich materials, carbonate-bearing surfaces, vegetation cover, and moisture conditions. Its 30 m multispectral resolution and improved radiometric resolution also make it suitable for baseline lithological assessment at the regional scale [5]–[8]. However, the usefulness of Landsat-based lithological discrimination is strongly conditioned by environmental context. In arid and semi-arid regions, exposed rock surfaces often produce clearer lithological contrasts, whereas in humid tropical landscapes, spectral separability is reduced by vegetation canopy, lateritic weathering, soil development, regolith cover, and mixed pixels [9]–[11].

Recent developments in lithological remote sensing increasingly emphasize multi-source data fusion and machine-learning classification to overcome the limitations of single-sensor optical imagery. Sentinel-2 data have been integrated with airborne gamma-ray spectrometric variables and Support Vector Machine classification to improve lithological separation in complex terrains [12], [13]. DEM-derived topographic variables have also been combined with Sentinel-2 imagery to enhance lithological classification where terrain morphology contributes to rock-unit separability [14]. More recent studies have further demonstrated the potential of optical–radar fusion, hyperspectral–multispectral comparison, automatic sample generation, and ensemble or deep-learning classifiers for rapid lithological mapping at broader spatial scales [15]–[18]. These developments indicate that high-confidence lithological mapping in complex landscapes increasingly relies on integrating spectral, topographic, geophysical, textural, and machine-learning information.

Nevertheless, classical optical enhancement and classification techniques remain scientifically relevant, particularly when the research objective is not to maximize classification accuracy through complex modelling, but to establish an interpretable and reproducible baseline. False-color composites can provide first-order visual separation of major surface materials; band ratios can enhance relative spectral differences and reduce illumination effects; Principal Component Analysis can compress redundant spectral information and highlight dominant variance structures; the Optimum Index Factor can support objective band selection; and Maximum Likelihood Classification remains a conventional benchmark for supervised multispectral classification. These methods are transparent, computationally efficient, and easier to interpret than many machine-learning models, making them useful for evaluating the minimum performance that can be expected from Landsat-9 OLI-2 alone [8], [11], [19], [20]. In this study, these classical methods are therefore not positioned as alternatives to contemporary machine-learning or multi-source approaches, but as a necessary baseline for assessing the realistic capability and limitations of optical multispectral data under dense tropical vegetation.

Langkawi Island, located in northwestern Peninsular Malaysia, provides a suitable and challenging test site for this purpose. The island contains a diverse assemblage of sedimentary, carbonate, granitic, and surficial units, and is characterized by persistent tropical vegetation cover and complex terrain. Previous studies in the Langkawi archipelago have shown that multispectral imagery and band-ratio techniques can support lithological interpretation, particularly in the Dayang Bunting and Tuba Islands, where limestone, marble, granite, and alluvial units can be visually enhanced using selected Landsat band combinations [2], [21]. However, those studies were spatially limited and did not evaluate the performance of classical Landsat-based methods across the whole of Langkawi Island. Extending the analysis to the island scale introduces additional complexity, including greater lithological heterogeneity, more continuous vegetation cover, stronger spectral mixing, broader transitions between carbonate, clastic, granitic, and alluvial units, and increased uncertainty in matching satellite-derived classes with published geological boundaries.

This study addresses that gap by developing a full-island, map-derived quantitative baseline for evaluating

Landsat-9 OLI-2 lithological discrimination in a densely vegetated tropical island environment. NDVI analysis indicates that dense vegetation covers 76.90% of Langkawi Island, while moderate-to-dense vegetation accounts for 92.82% of the mapped area. Under these conditions, Landsat-9 OLI-2 reflectance should be interpreted as a mixed surface response rather than a direct lithological signal. Consequently, evaluating the agreement between satellite-derived lithological classes and the published geological map is important not only for measuring classification performance but also for identifying the specific lithological confusions caused by vegetation cover, tropical weathering, mixed pixels, spatial resolution and reference-map uncertainty.

Therefore, this study aims to establish a full-island, map-derived quantitative baseline for evaluating the applicability and limitations of Landsat-9 OLI-2 in lithological discrimination on Langkawi Island. The specific objectives are to: (1) evaluate the capability of classical Landsat-9 OLI-2 enhancement techniques, including false-color composites, OIF-based band selection, band-ratio composites, and PCA, to enhance major lithological contrasts; (2) assess the map-derived agreement between the MLC-derived lithological classification and the published geological map; (3) examine how NDVI-defined vegetation-cover classes influence lithological agreement; and (4) identify the dominant lithological class confusions and interpret their possible causes in relation to vegetation cover, tropical weathering, mixed pixels, Landsat spatial resolution, and reference-map uncertainty.

2. LITERATURE BACKGROUND

Remote-sensing-based lithological mapping has long relied on optical multispectral imagery because visible, near-infrared, and short-wave infrared bands can capture surface reflectance variations related to mineral composition, weathering products, soil cover, moisture conditions, and geomorphological expression. Landsat data remain widely used in geological applications because they are freely available, spatially continuous, and suitable for regional-scale lithological interpretation. Recent Landsat- and ASTER-based studies show that image enhancement and classification techniques can support lithological discrimination in different geological settings [10], [22]. In the Langkawi archipelago, previous work demonstrated the usefulness of multispectral band-ratio techniques for enhancing lithological contrasts in selected local areas [2], [21].

Classical multispectral techniques remain relevant because they are interpretable, computationally simple, and easy to reproduce. Band ratios and PCA are frequently used to enhance lithological contrasts and reduce spectral redundancy before classification [8], [10], [22]. OIF provides a statistical basis for selecting informative three-band combinations by considering information content and inter-band redundancy; although originally proposed by Chavez et al. [20], it continues to be used together with FCC, band ratioing, PCA, and MNF in lithological mapping workflows [23]. MLC remains useful as a benchmark classifier because it allows the baseline separability of lithological classes to be evaluated and compared with more advanced classifiers such as SVM [22], [24]. These methods are therefore suitable when the objective is to establish a transparent Landsat-based baseline rather than to develop an optimized machine-learning classification model.

However, optical-only lithological mapping has important limitations in humid tropical and vegetation-covered regions. Dense vegetation, weathered regolith, soil cover, topographic shadow, and mixed pixels can weaken or mask bedrock-related spectral responses. This issue is particularly relevant to Langkawi Island, where sedimentary, carbonate, granitic, and alluvial units occur under persistent tropical vegetation cover. Recent studies indicate that classification performance and class-level separability are strongly influenced by spectral overlap among lithological units and by the availability of independent validation evidence [7], [12], [14], further emphasized that vegetation-covered regions remain among the most difficult environments for lithological mapping because vegetation and surface materials can obscure diagnostic spectral information, while Chen et al. [16] showed that lithological mapping in high-vegetation areas can benefit from integrating optical imagery with Sentinel-1 SAR and DEM data.

Recent studies have increasingly adopted multi-source data fusion and machine-learning approaches to address these limitations. Shebl et al. [26] integrated Sentinel-2 imagery with gamma-ray spectrometric data and SVM classification, showing that combining optical reflectance with geophysical information can improve lithological discrimination in complex terrains. Shebl et al. [14] demonstrated that DEM-derived variables can improve Sentinel-2-based lithological mapping by incorporating terrain-related information. Optical-radar fusion has also become an important direction, as radar data can provide structural and surface-roughness information complementary to optical reflectance, as shown in recent studies using both optical and radar data for geological and lithological mapping [18]. In addition, machine-learning models such as Random Forest, SVM, gradient boosting, extreme gradient boosting, and artificial neural networks have increasingly been used to model non-linear relationships among spectral, topographic, textural, and geological variables [15], [17], [27]. More broadly, intelligent lithological mapping is moving toward artificial intelligence, multi-source geospatial data fusion, cloud computing, uncertainty quantification, and model interpretability [28].

Although these recent studies demonstrate the advantages of multi-source data and machine-learning approaches, they also highlight the need for simpler, more

interpretable baseline assessments. For Langkawi Island, previous studies have mainly examined localized areas of the archipelago rather than the whole island [2], [21]. As a result, it remains unclear how well classical Landsat-based methods perform at the full-island scale, where lithological heterogeneity, vegetation cover, weathering, mixed pixels, and transitional boundaries are more pronounced. The present study, therefore, does not seek to replace optical-radar-DEM fusion or machine-learning methods. Instead, it provides a full-island Landsat-9 OLI-2 baseline for identifying which lithological units are broadly separable, which units remain confused, and which environmental factors limit classification performance in a humid tropical island setting.

In humid tropical lithological mapping, classification performance is controlled not only by bedrock composition but also by the surface materials that dominate the sensor signal. Dense vegetation can mask lithological reflectance; regolith and weathered soils can produce secondary spectral responses that differ from those of fresh bedrock; and mixed pixels at 30 m resolution often contain vegetation, soil, rock fragments, and anthropogenic surfaces simultaneously. Therefore, spectral separability in Landsat imagery should be interpreted as the separability of surface expressions associated with lithological units rather than the direct separability of bedrock lithology itself.

Taken together, previous studies can be organized into four methodological directions relevant to the present study. First, image-enhancement methods such as FCC, band ratios, OIF, and PCA are useful for highlighting broad spectral and surface-material contrasts, but they do not independently validate lithological boundaries. Second, supervised classifiers such as MLC, SVM, and RF assign pixels to lithological classes, but their reliability depends on training samples, class separability, surface heterogeneity, and assessment design.

Third, multi-source approaches using Sentinel-1 SAR, DEM-derived variables, gamma-ray data, or higher-resolution optical imagery can improve lithological discrimination by adding structural, terrain, or geophysical information beyond optical reflectance. Fourth, assessment strategies differ substantially: independent field validation provides stronger evidence of lithological accuracy, whereas comparison with an existing geological map provides map-derived agreement. The present study is positioned within this framework as a transparent optical-only baseline assessment that evaluates Landsat-9 OLI-2 enhancement capability, MLC-based map-derived agreement, NDVI-related surface-cover effects, and major class confusion under humid tropical vegetation conditions.

3. GEOLOGICAL SETTINGS

The Langkawi Archipelago, situated in the Andaman Sea off the northwestern coast of Peninsular Malaysia, comprises 104 islands, approximately 30 km west of Perlis and 112 km north of Penang (Figure 1). This archipelago is geologically significant because it exposes one of Malaysia's oldest and most complete Paleozoic sedimentary successions, making it a key reference area for reconstructing the stratigraphic and tectonic evolution of northwestern Peninsular Malaysia [29]–[31].

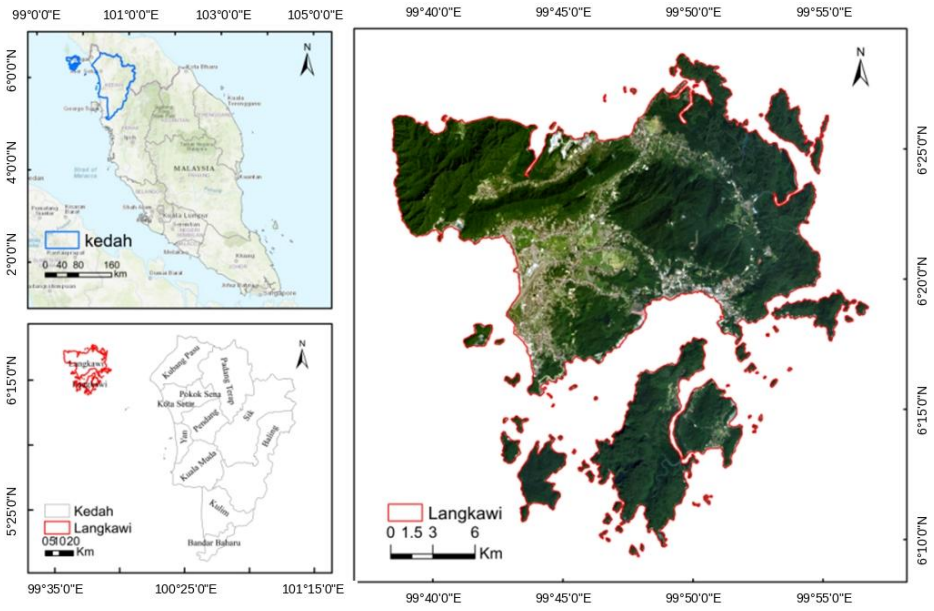

Figure 1. The Langkawi study area is located in the northwestern part of Peninsular Malaysia.

Langkawi Island is underlain by a heterogeneous lithological framework comprising Paleozoic sedimentary successions, Mesozoic granitic intrusions, and Quaternary unconsolidated deposits (Figure 2). The sedimentary succession ranges from Cambrian to Triassic age and records a transition from siliciclastic deposition

to carbonate-platform development and glacial-marine sedimentation under varied paleogeographic and paleoclimatic conditions [31]–[34]. This lithological diversity is further complicated by the emplacement of granitic bodies and the accumulation of younger alluvial deposits, which together shape the geomorphological and spectral complexity of the study area.

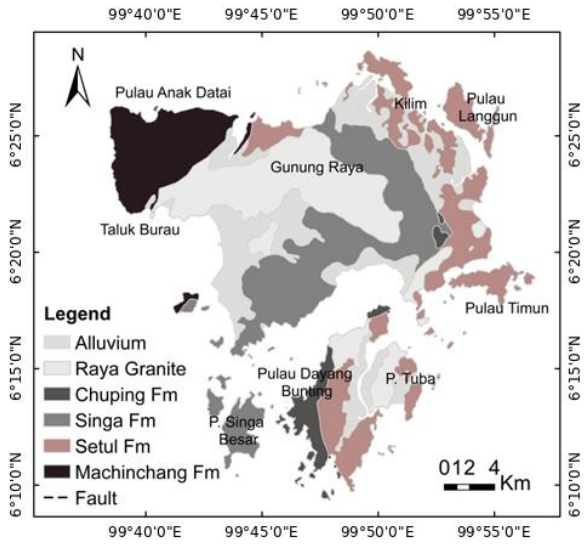

Figure 2. Geological map of Langkawi Island showing the distribution of its varied rock formations [35].

The main geological units exposed in Langkawi comprise the Machinchang Formation, Setul Formation, Singa Formation, Chuping Formation, Gunung Raya Granite, and Quaternary Alluvium [35]. These units respectively represent sandstone–shale–mudstone assemblages, carbonate and carbonate-clastic formations, dark siltstone–mudstone successions, intrusive granitic terrain, and unconsolidated surficial deposits [29], [30]. Such lithological variation provides an important geological basis for evaluating surface reflectance patterns and lithological discrimination using multispectral remote-sensing data.

These lithological units provide the geological framework for interpreting Landsat-derived spectral responses because rock composition, mineralogy, weathering intensity, geomorphological expression, and vegetation cover jointly control surface reflectance. However, lithological separability cannot be inferred from bedrock type alone, particularly in humid tropical environments where dense vegetation, regolith development, soil moisture, and mixed pixels frequently obscure primary lithological signals [36], [37]. Therefore, Table 1 summarizes the main lithological units in Langkawi and their expected remote-sensing relevance, serving as a basis for interpreting Landsat 9 OLI-2 outputs.

Table 1. Langkawi lithology descriptions.

No	Stratigraphic Formation	Lithology description	Remote-sensing relevance
1	Machinchang Formation (Cambrian) Cm-SS/Sh/Md	Sandstone, shale, and mudstone	Textural variation may be visible in exposed or sparsely vegetated areas, but spectral overlap may occur under vegetation and in weathered areas.
2	Setul Formation (Ordovician to Silurian) OS-Ls/SS	Limestone and sandstone	Carbonate-clastic composition may show SWIR-related contrast, but can overlap with other carbonate-bearing units.
3	Singa Formation (Devonian to Permian) DP-St/Md	Dark siltstone and mudstone	Fine-grained dark lithology may be difficult to separate due to soil, regolith, and vegetation cover.
4	Chuping Formation (Permian to Triassic) PT-Ls/Mb	Thin limestone, sometimes transformed into marble	Carbonate-bearing surfaces may be spectrally similar to OS-Ls/SS under weathering and vegetation cover.
5	Gunung Raya Granite (Triassic) Tr-Gr	Granite (intrusive, tectonically uplifted)	Granitic terrain may be influenced by upland topography, vegetation, and weathered granitic regolith.
6	Alluvium (Quaternary) Qal	Unconsolidated Alluvium	Lowland and coastal settings may support detection, but confusion with exposed soil, agriculture, and weathered materials is possible.

Note. Cm = Cambrian, O = Ordovician, S = Silurian, D = Devonian, P = Permian, T = Triassic, Q = Quaternary, SS = Sandstone, Sh = Shale, Md = Mudstone, Ls = Limestone, St = Siltstone, Mb = Marble, Gr = Granite, al = Alluvium.

From a multispectral perspective, Quaternary Alluvium is expected to be relatively more distinguishable because its lowland and coastal distribution contrasts with the upland bedrock terrain. Granitic areas may also be identifiable through their combined geomorphological expression, topographic position, and weathered regolith characteristics, although vegetation cover can reduce direct spectral contrast. In contrast, carbonate-bearing units such as the Setul and Chuping formations may produce responses similar to those of shortwave-infrared reflectance under weathered or vegetated conditions. In contrast, fine-grained clastic units such as the Singa Formation may show weak separability due to their low albedo and frequent association with soil, shadow, and vegetation. Consequently, Landsat 9 OLI-2 is considered more appropriate for broad lithological-domain discrimination than for precise formation-level separation in the humid tropical setting of Langkawi [38]–[40].

4. MATERIALS AND METHODS

4.1. Satellite Data

This study used two Landsat-9 OLI-2/TIRS-2 scenes acquired from the United States Geological Survey (USGS) to cover the Langkawi Island study area. The images were acquired on 7 December 2021 and 15 January 2022, respectively. Both datasets are Level-1 terrain-corrected products with high geometric quality. For lithological analysis, this study used the reflective Landsat-9 OLI-2 multispectral Bands 1-7, which cover the coastal/aerosol, visible, near-infrared, and short-wave infrared regions at 30 m spatial resolution (Table 2). Bands 8-11 were not used because the panchromatic, cirrus, and thermal bands were not required for the multispectral lithological enhancement and classification procedures applied in this study.

The two scenes were acquired approximately six weeks apart. Although this short interval reduced seasonal differences, potential variations in vegetation greenness, surface moisture, tidal conditions, illumination geometry, and atmospheric conditions could not be eliminated. To minimize these effects, both scenes were processed using the same radiometric calibration and atmospheric correction workflow prior to mosaicking. After atmospheric correction, the mosaic was visually inspected to identify obvious radiometric discontinuities across scene boundaries and adjacent stable areas. No major discontinuity was observed that would prevent its use for island-scale lithological interpretation. Because independent field spectral measurements were not available, the final mosaic was used to establish a map-derived baseline rather than to produce a field-validated lithological map.

Table 2. Landsat 9 data band ranges and spatial resolution.

Band	Band Description	Wavelength Range (μm)	Spatial Resolution (m)	Band	Band Description	Wavelength Range (μm)	Spatial Resolution (m)
1	Coastal/Aerosol	0.43 - 0.45	30	Band 7	Short infrared	2.10 - 2.29	30
2	Visible blue	0.45 - 0.51	30	Band 8	Panchromatic	0.50 - 0.67	15
3	Visible green	0.53 - 0.59	30	Band 9	Cirrus	1.36 - 1.38	30
4	Visible red	0.63 - 0.67	30	Band 10	Thermal infrared	10.60 - 11.19	100
5	Near-infrared	0.85 - 0.87	30	Band 11	Thermal infrared	11.50 - 12.51	100
6	Short infrared	1.56 - 1.65	30				

Table 3. Landsat-9 scenes used in this study

Scene ID	Acquisition date	Path/Row	Processing level	Cloud Cover (%)
LC91280562021341LGN01	07/12/2021	128/056	Level-1 TP	6.7%
LC91290552022015LGN02	15/01/2022	129/055	Level-1 TP	0.05%

4.2. Pre-processing

The Landsat-9 OLI-2 scenes used in this study were Level-1 terrain-corrected products obtained from the United States Geological Survey. These products had already undergone systematic radiometric and geometric processing, including precision and terrain corrections to improve geometric accuracy. Therefore, the pre-processing in this study focused on radiometric calibration, atmospheric correction, layer stacking, mosaicking, and sub-setting. Similar pre-processing workflows, including radiometric calibration, atmospheric correction, surface-reflectance generation, band stacking, and image enhancement, have been widely adopted in Landsat-based geological and lithological mapping studies [41], [42].

In ENVI 5.3, the Landsat-9 OLI-2 scenes were radiometrically calibrated from digital numbers to at-sensor radiance and atmospherically corrected to surface reflectance using the FLAASH module. The Tropical atmospheric model was selected to represent the humid equatorial conditions of Langkawi Island.

After atmospheric correction, the OLI-2 bands used for lithological analysis were stacked. Because two adjacent Landsat-9 scenes covered Langkawi Island, the corrected scenes were mosaicked after atmospheric correction to reduce radiometric inconsistency between scenes and then clipped to the Langkawi Island boundary. Obvious cloud- and shadow-affected areas were visually checked during image preparation and interpretation. Because the selected scenes had low cloud cover, no extensive cloud-masking procedure was required for the main lithological analysis. The mosaic was also visually inspected along scene boundaries and adjacent stable surfaces to identify any obvious radiometric discontinuity. No major discontinuity was observed that would prevent the use of the mosaic for island-scale lithological interpretation.

The processed surface-reflectance dataset was subsequently used for NDVI calculation, false-color composite generation, band-ratio analysis, OIF calculation, PCA, and MLC-supervised classification. The overall workflow is shown in Figure 3.

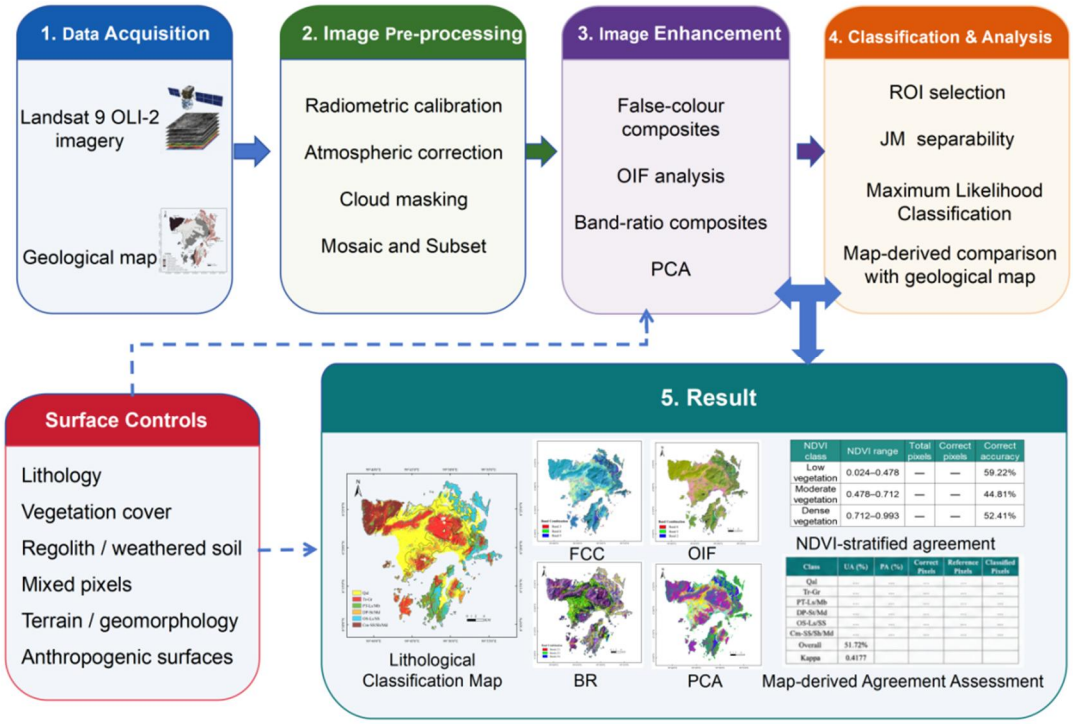

Figure 3. Integrated methodological and conceptual framework for Landsat-9 OLI-2-based lithological discrimination in Langkawi Island.

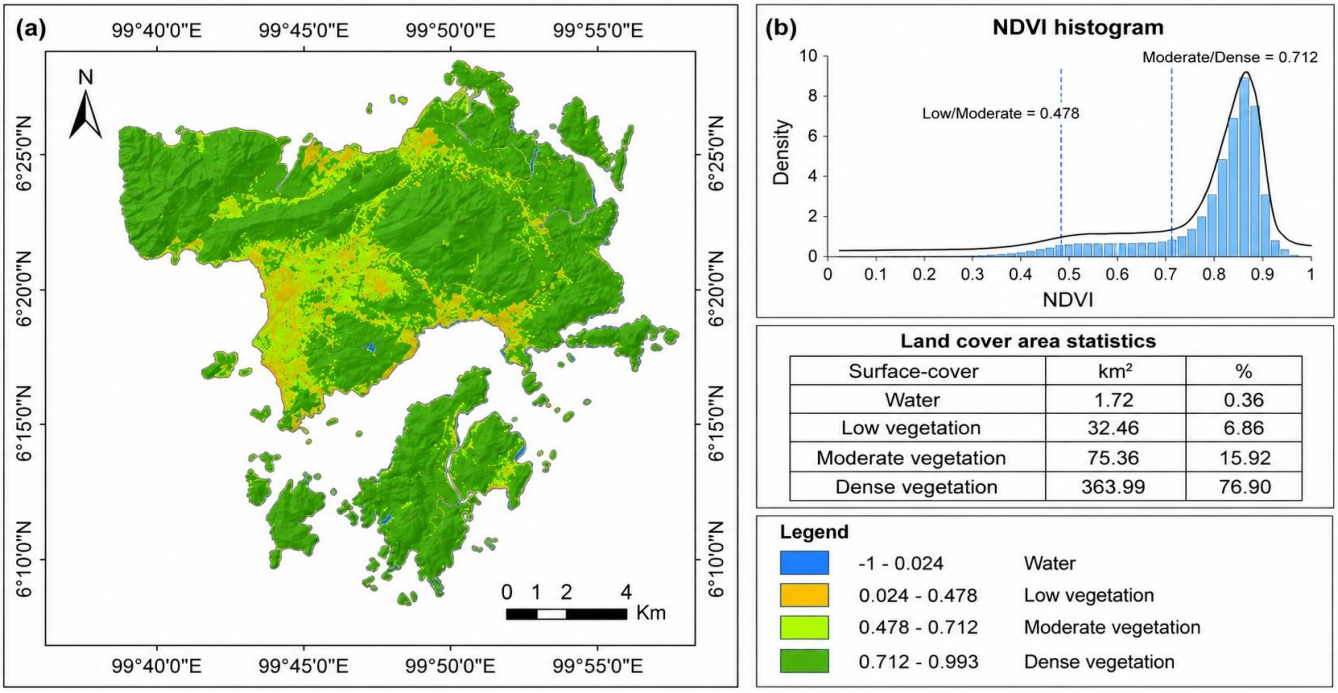

Figure 4. NDVI-derived land-cover classification of the study area. (a) Spatial distribution of water and vegetation classes based on NDVI thresholds. (b) NDVI histogram showing the class separation thresholds at 0.478 and 0.712.

To characterize the surface-cover context of the study area, a Normalized Difference Vegetation Index (NDVI) image was generated from atmospherically corrected Landsat-9 OLI-2 data using Bands 5 (near-infrared) and 4 (red), following the standard formula [43].

In Equation (1), NDVI denotes the Normalized Difference Vegetation Index, whereas NIR and Red refer to the reflectance values of the near-infrared and red spectral bands, respectively. In Landsat 8 imagery, these bands correspond to Band 5 and Band 4. NDVI values range from -1 to +1, with higher positive values indicating

dense vegetation, near-zero values representing bare surfaces or exposed rocks, and negative values commonly associated with water bodies or non-vegetated features.

$$\mathrm{NDVI}=\frac{(\mathrm{NIR}-\mathrm{Red})}{(\mathrm{NIR}+\mathrm{Red})} \quad (1)$$

The NDVI image was used to describe the surface-cover context of Langkawi Island rather than as an independent land-cover classification product. Based on the NDVI histogram, image patterns, and general surface-cover characteristics, water pixels were excluded and the remaining land pixels were grouped into low-, moderate-, and dense-vegetation classes using thresholds of 0.478 and 0.712 (Figure 4).

These classes were used as generalized vegetation-cover strata. Low-vegetation areas may include exposed soil, regolith, agricultural surfaces, settlement margins, and sparsely vegetated lithological surfaces. In contrast, moderate-vegetation areas may contain mixed pixels composed of vegetation, soil, weathered materials, and anthropogenic surfaces. Therefore, the NDVI-stratified analysis was used to evaluate general vegetation-related effects on map-derived lithological agreement rather than treating vegetation as the sole controlling factor.

To further examine the influence of vegetation cover on map-derived lithological agreement, an NDVI-stratified agreement assessment was conducted. Water pixels were excluded from the lithological agreement assessment. The MLC classification map and the reference geological map were first converted to a common lithological code system. A binary agreement raster was generated, with pixels having matching lithological codes assigned a value of 1 and mismatched pixels assigned a value of 0. The mean agreement raster value within each NDVI class was multiplied by 100 to obtain map-derived agreement (%).

4.3. Band Ratio (BR)

Band ratioing is a widely used multispectral enhancement technique for lithological discrimination because it emphasizes relative spectral differences between surface materials while reducing the effects of illumination, topographic shading, and other scene-dependent variations [44], [45]. In geological applications, it is particularly useful for enhancing broad lithological contrasts and improving the visual separability of major rock units [11].

In this study, two band-ratio combinations, (5/3, 6/4, 5/4) and (2/3, 2/5, 2/6), were selected based on previous lithological remote-sensing studies in the Langkawi archipelago and comparable multispectral geological applications [2], [21]. Therefore, the purpose was not to optimize all possible band-ratio combinations, but to evaluate whether previously reported ratio schemes remain useful when applied to a full-island Landsat-9 OLI-2 baseline assessment.

These combinations include visible, near-infrared, and shortwave-infrared bands, which are relevant to vegetation condition, surface moisture, weathered materials, clay-bearing surfaces, carbonate-bearing formations, and silica-rich or clastic lithological expressions. Therefore, the ratio images were interpreted as regional lithological enhancement products rather than as direct diagnostic evidence of bedrock lithology.

4.4. Optimum Index Factor (OIF)

OIF was used to identify the most informative three-band combination for generating false-color composites, following Chavez et al. [20]. Higher OIF values indicate greater information content and lower redundancy [46]. OIF values were calculated for all possible three-band combinations of the Landsat-9 imagery in ILWIS, and the highest-ranked combination was selected for visual lithological interpretation. The optimal combination for the study area was RGB 6-5-2.

4.5. Principal Component Analysis (PCA)

Principal Component Analysis (PCA) is a widely used multivariate technique in remote sensing that transforms correlated spectral bands into a new set of orthogonal and uncorrelated variables, thereby reducing dimensionality and spectral redundancy [22], [23]. The first principal component contains the largest proportion of total variance, whereas subsequent components account for progressively smaller amounts; higher-order components are often dominated by noise [47]. Because PCA concentrates most spectral information into a limited number of components, it is widely used to enhance interpretability and support lithological and mineralogical mapping [48], [49].

4.6. Maximum Likelihood Classification (MLC)

MLC was applied to the atmospherically corrected Landsat-9 OLI-2 reflective bands to produce an island-scale lithological classification of Langkawi Island. MLC assigns pixels to classes based on class statistics and probability distributions, and it remains a widely used benchmark classifier in multispectral remote sensing and lithological mapping studies [50]–[52]. The classification classes followed the generalized lithological units listed in Table 1.

Training ROIs were delineated with reference to the published geological map, false-color composites, band-ratio images, PCA products, and previous remote-sensing interpretations. Relatively homogeneous areas were prioritized, while water bodies, cloud-affected pixels, strongly mixed boundary zones, and obvious non-lithological surfaces were avoided where possible. Table 4 summarizes the distribution of training ROI pixels for each lithological class used in the MLC.

The MLC-derived lithological classification was evaluated by comparing the map with the published

geological map of Langkawi Island. Before comparison, both maps were converted into the same lithological code system, and a confusion matrix was generated from the pixel-by-pixel comparison. Map-derived agreement, producer's [53] agreement, user's agreement, F1-score, and the kappa coefficient were calculated from the reference-map comparison following standard confusion-matrix procedures [17], [53]. However, because the comparison was based on the published geological map rather than independent field samples, these values were interpreted as map-derived agreement statistics rather than independent field-based lithological accuracy.

Because independent field validation samples were not available, the published geological map served as the reference framework for the map-derived agreement assessment. Since the same geological framework also informed ROI selection, the assessment was not fully independent. Therefore, the reported agreement values should be interpreted as map-derived agreement with the existing geological framework rather than field-validated lithological accuracy. The MLC result was treated as a reconnaissance-level baseline classification product for evaluating the applicability and limitations of classical Landsat-9 OLI-2 lithological discrimination under dense tropical vegetation cover.

Table 4. Distribution of training ROI pixels for each lithological class.

No.	Lithological class	Training ROI pixels
1	Cm-SS/Sh/Md	1,442
2	OS-Ls/SS	3,271
3	DP-St/Md	1,163
4	PT-Ls/Mb	1,686
5	Tr-Gr	2,773
6	Qal	1,815
Total		12,150

Separability analysis was conducted after selecting the training samples to assess spectral differences among the lithological classes. Following previous remote-sensing classification studies, the Jeffries–Matusita (JM) distance was used to evaluate the statistical separability between class pairs [12], [54]. The JM distance ranges from 0 to 2, with values closer to 2 indicating stronger separability. The pairwise JM distance matrix is presented in Table 5.

Table 5. Pairwise Jeffries–Matusita separability matrix for lithological training ROIs.

Class	Cm-SS/Sh/Md	OS-Ls/SS	DP-St/Md	PT-Ls/Mb	Tr-Gr	Qal
Cm-SS/Sh/Md	2.000	2.000	1.998	2.000	1.922	1.992
OS-Ls/SS		2.000	1.924	1.807	1.931	1.999
DP-St/Md			2.000	1.892	1.868	1.979
PT-Ls/Mb				2.000	1.909	1.998
Tr-Gr					2.000	1.926
Qal						2.000

Table 5 shows that most class pairs had high separability, with JM values close to 2.000, indicating that the selected training ROIs were generally suitable for supervised classification. However, several class pairs showed relatively lower separability, including OS-Ls/SS vs PT-Ls/Mb (1.807), DP-St/Md vs Tr-Gr (1.868), DP-St/Md vs PT-Ls/Mb (1.892), PT-Ls/Mb vs Tr-Gr (1.909), and Cm-SS/Sh/Md vs Tr-Gr (1.922). These relatively lower values suggest potential spectral overlap among carbonate-bearing units, fine-grained sedimentary units, and weathered granitic surfaces. Therefore, the separability analysis was used not only to assess the suitability of the training samples but also to support the interpretation of class-level confusion in the MLC results.

5. RESULTS

5.1. False-color Composites

False-color composites derived from Landsat-9 OLI-2 imagery were used to provide a first-order view of the spatial distribution of major surface materials across Langkawi Island. Both literature-based and quantitative criteria guided the selection of band combinations. First, RGB 3-6-5, 7-4-2, and 5-6-7 composites were generated based on previous lithological and geological remote sensing studies [55], [56].

Table 6. Optimum Index Factor Ranking for Landsat OLI-2.

Ranking	Band 1	Band 2	Band 3	OIF Value
1	b6	b5	b2	1112.8
2	b4	b5	b6	1079.48
3	b1	b5	b6	1070.7
4	b5	b6	b7	1053.65
5	b3	b5	b6	1009
6	b2	b5	b7	986.65

These combinations were selected because they include visible, near-infrared, and shortwave-infrared bands that are useful for enhancing differences in vegetation cover, exposed bedrock, surface moisture, alluvial materials, and lithological variations. Second, the Optimum Index

Factor (OIF) was calculated to quantitatively evaluate possible three-band combinations according to their information content and inter-band redundancy. The OIF analysis identified RGB 6-5-2 as the optimal combination, with an OIF value of 1112.80 (Table 6), indicating high information content and relatively low inter-band redundancy. However, OIF was used only as a statistical band-selection tool and should not be interpreted as direct proof of lithological separability.

The false-color composites derived from different band combinations reveal distinguishable lithological and surface-material patterns across the study area. In the RGB 3-6-5 composite (Figure 5a), dark blue tones indicate alluvial deposits, whereas light yellow and green tones represent Alluvium converted to settlement or agricultural land; blue-toned areas with clear texture correspond to bedrock outcrops [46]. In the RGB 7-4-2 composite (Figure 5b), purple represents Alluvium, grey indicates bedrock, and yellow corresponds to settlement and agricultural areas [55]. The RGB 5-6-7 composite (Figure 5c) shows Alluvium in red, geologically distinct units in various khaki shades, and anthropogenically modified land in cyan [4]. The OIF-selected RGB 6-5-2 composite (Figure 5d), which integrates shortwave-infrared, near-infrared, and visible bands, shows Alluvium in deep green, bedrock as a light-to-dark green gradient, and agriculture and settlement in rose tones.

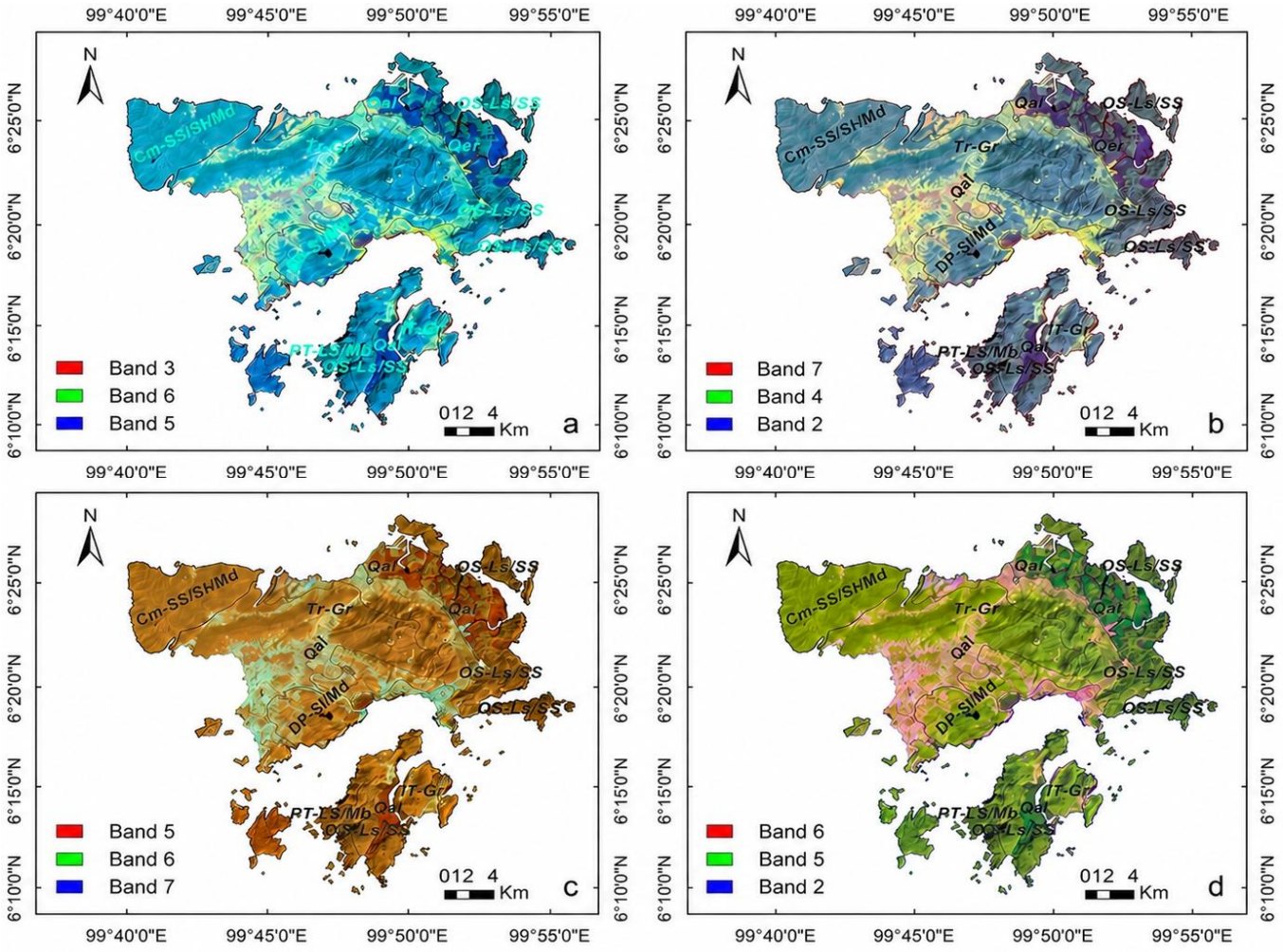

Figure 5. False-color composites of Landsat-9 OLI-2 imagery. (a) RGB 3-6-5; (b) RGB 7-4-2; (c) RGB 5-6-7; (d) RGB 6-5-2.

The comparison shows that the literature-based composites are useful for interpreting previously reported lithological and land-cover patterns. In contrast, the OIF-selected RGB 6-5-2 composite provides an additional statistically supported band combination with relatively high information content. The final interpretation, therefore, considered both the geological relevance of previously reported band combinations and the quantitative OIF ranking, rather than relying solely on visual inspection. In the OIF-selected RGB 6-5-2 composite, Band 6 captures SWIR reflectance variations related to moisture, clay-bearing weathering products, and lithological surface materials; Band 5 captures vegetation and near-infrared surface response; and Band 2 contributes visible reflectance contrast. However, this composite was used only as a regional enhancement product, not as direct proof of lithological separability.

5.2. Band Ratio

The selected band-ratio composites, 5/3-6/4-5/4 and 2/3-2/5-2/6, were generated based on previous lithological mapping studies in the Langkawi archipelago and similar geological settings [2], [21]. These ratio combinations were selected because they involve visible, near-infrared, and shortwave infrared bands that are sensitive to variations in vegetation condition, surface moisture, clay-bearing materials, and carbonate- or silica-rich lithological surfaces. Therefore, they are useful for enhancing relative spectral contrasts among major lithological groups and for providing supplementary lithological information beyond the original multispectral composites.

The band-ratio composites enhanced broad spectral differences among granitic terrain, carbonate-bearing formations, and Quaternary alluvium (Figure 6). Qal showed relatively distinctive and spatially consistent responses in both composites, reflecting its lowland alluvial setting. In contrast, PT-Ls/Mb and OS-Ls/SS showed similar spectral responses, indicating overlap between carbonate-bearing and carbonate–clastic surfaces under vegetation and weathering conditions (Figure 6 a,b). Cm-SS/Sh/Md showed textural features but partially overlapped with Tr-Gr. Therefore, the selected ratio schemes were useful for enhancing broad lithological contrasts, but their interpretation should be integrated with geological context and separability analysis rather than used as direct diagnostic evidence.

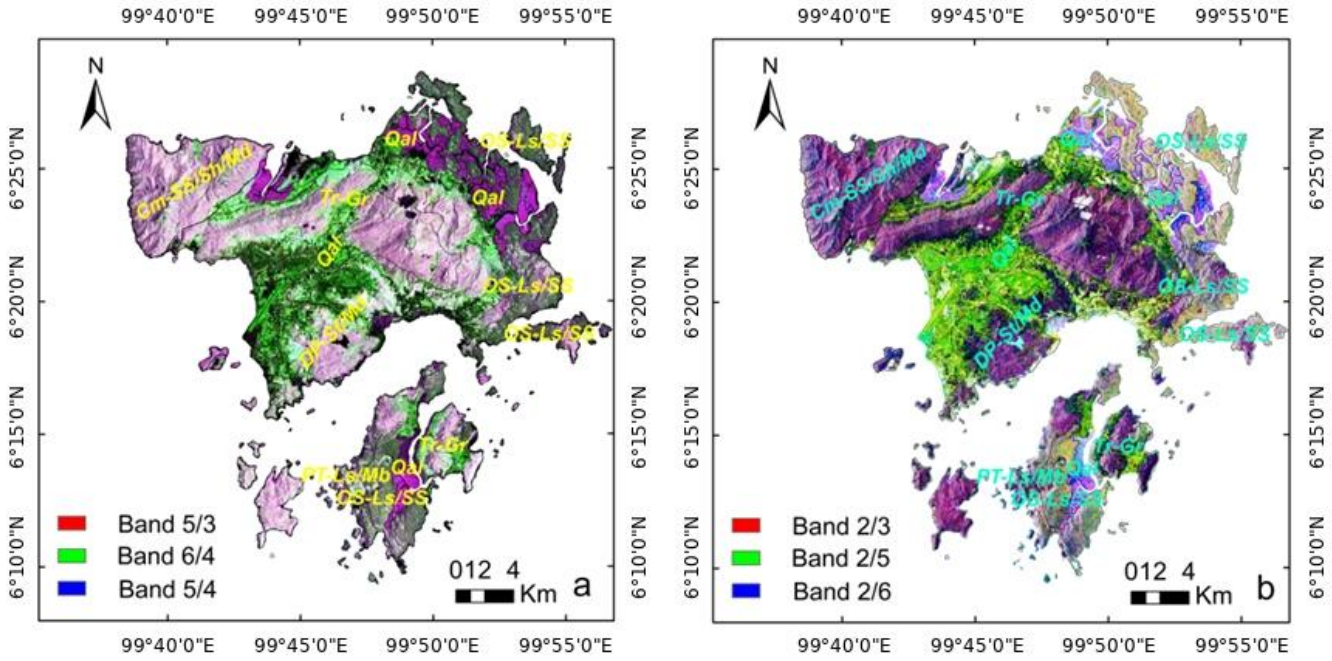

Figure 6. Landsat-9 OLI-2 band-ratio composites used for lithological enhancement (a) RGB 5/3–6/4–5/4 and (b) RGB 2/3–2/5–2/6.

Table 7. PCA Eigenvectors matrix of the PCA calculated for Landsat OLI-2 data.

Bands/PC	PC1	PC2	PC3	PC4	PC5	PC6	PC7
Eigenvalues %	92.555	6.251	1.064	0.073	0.044	0.011	0.002
Band 1	0.165	0.069	-0.514	0.003	-0.530	0.290	0.582
Band 2	0.143	0.102	-0.472	-0.026	-0.308	0.103	-0.800
Band 3	0.193	0.111	-0.456	-0.183	0.224	-0.801	0.134
Band 4	0.179	0.273	-0.334	-0.026	0.734	0.490	0.046
Band 5	**0.769**	**-0.612**	0.092	0.138	0.067	0.033	-0.020
Band 6	0.470	0.507	0.404	**-0.575**	-0.164	0.038	-0.003
Band 7	0.264	**0.516**	0.149	**0.785**	-0.064	-0.146	0.006

Note. Bold values indicate dominant band loadings for each principal component.

5.3. Principal Component Analysis (PCA)

The principal component analysis (PCA) results derived from Landsat OLI-2 imagery (Table 7) and illustrated in Figure 7. PCA was applied to the atmospherically corrected Landsat-9 OLI-2 reflective Bands 1-7 to reduce spectral redundancy and enhance dominant spectral patterns related to lithological and surface-cover variation. The eigenvalue contribution in Table 7 shows

that most spectral variance was concentrated in PC1 and PC2. The first three components accounted for most of the total variance: PC1, 92.555%; PC2, 6.251%; and PC3, 1.064%. PC1 mainly represents overall surface brightness, vegetation-related reflectance, and illumination variation because all reflective bands contributed positively. PC2 enhances contrast between near-infrared and shortwave-infrared responses, making it useful for interpreting broad differences among vegetation-covered surfaces, carbonate-bearing formations, and granitic terrains. PC3 mainly captures additional visible-band variation and provides limited supplementary information for alluvial and exposed surface materials.

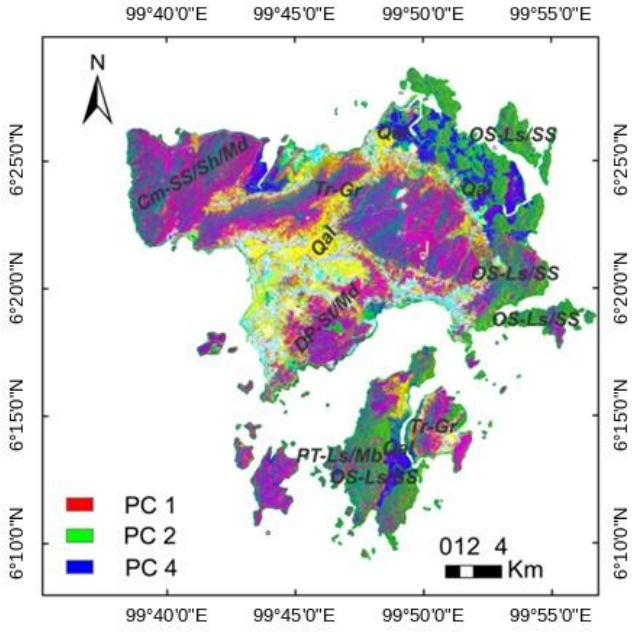

Figure 7. RGB composite of PC1, PC2, and PC4. PC1 explains 92.555% of the variance, PC2 explains 6.251%, and PC4 explains 0.073%.

Although PC4 explained only 0.073% of the total variance, it was retained in the PC1, PC2, and PC4 RGB composite as a supplementary enhancement layer because it locally enhances SWIR-related contrast between carbonate-bearing and granitic terrains. Therefore, PC4 was interpreted cautiously and was not used as an independent basis for lithological discrimination. The PC1, PC2, and PC4 composites provide an interpretable PCA product for regional lithological analysis, especially for broad contrasts among Alluvium, granitic terrain, and carbonate-bearing areas. However, local spectral mixing remains evident in vegetation-covered zones and along lithological transitions, indicating that PCA can enhance dominant lithological patterns but cannot fully resolve spectral overlap among formations with similar surface composition or limited bedrock exposure.

5.4. Maximum Likelihood Classification (MLC)

The MLC-derived lithological classification reproduced some broad regional lithological patterns, but substantial class confusion remained when compared with the reference geological map (Figure 8a,b). Compared with previous localized studies in Langkawi and nearby islands, the present island-scale classification showed stronger confusion among PT-Ls/Mb, OS-Ls/SS, and DP-St/Md, highlighting the influence of larger spatial extent, greater lithological heterogeneity, dense vegetation cover, and more complex surface conditions on multispectral lithological mapping performance [2], [21].

The MLC-derived lithological classification achieved an overall map-derived agreement of 51.72% and a kappa coefficient of 0.4177, indicating moderate agreement with the reference geological map (Table 8). Class-level agreement varied substantially. Qal showed the highest producer's agreement (90.21%) but only moderate user's agreement (50.63%), indicating notable commission error. OS-Ls/SS had the highest user's agreement (74.93%), whereas DP-St/Md showed the lowest producer's agreement (23.09%) and was strongly confused with Qal and Tr-Gr. PT-Ls/Mb also showed severe commission error, with a very low user's agreement of 17.34%, especially in areas corresponding to OS-Ls/SS and DP-St/Md.

Table 8. Confusion matrix and class-level map-derived agreement statistics for the MLC-derived lithological classification.

Classified class	Qal	Tr-Gr	PT-Ls/Mb	DP-St/Md	OS-Ls/SS	Cm-SS/Sh/Md	Total	UA (%)
Qal	72,267	23,142	516	35,329	9,993	1,495	142,742	50.63
Tr-Gr	232	45,620	1,964	24,880	6,262	8,666	87,624	52.06
PT-Ls/Mb	2,326	7,894	10,245	11,518	21,903	5,179	59,065	17.34
DP-St/Md	2,149	15,741	656	25,859	4,590	2,497	51,492	50.22
OS-Ls/SS	2,699	5,079	2,090	5,280	48,651	1,127	64,926	74.93
Cm-SS/Sh/Md	437	7,712	362	9,103	2,645	36,775	57,034	64.48
Total	80,110	105,188	15,833	111,969	94,044	55,739	462,883	
PA (%)	90.21	43.37	64.71	23.09	51.73	65.98		
F1-score (%)	64.86	47.32	27.35	31.63	61.21	65.22		

Note. Values represent pixel counts. Rows indicate MLC-classified lithological classes, whereas columns indicate reference geological-map classes. UA = user's agreement; PA = producer's agreement. These values represent class-level map-derived agreement statistics based on reference-map comparison rather than independent field-based lithological accuracy. Map-derived agreement = 51.72%; Kappa coefficient = 0.4177.

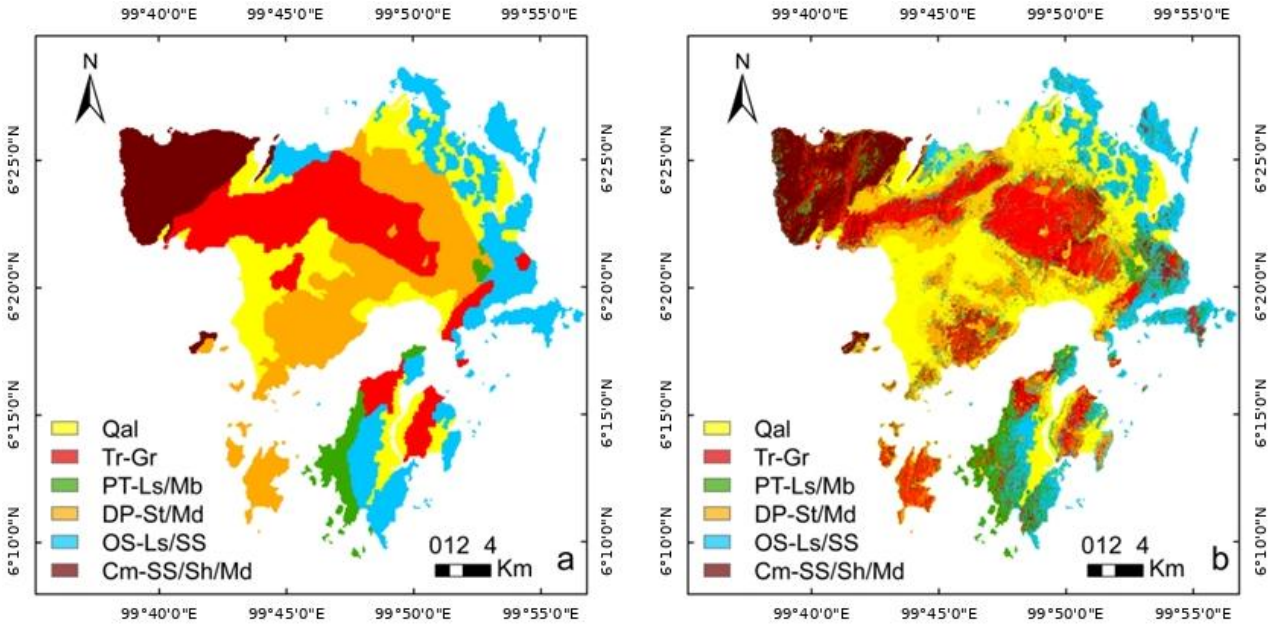

Figure 8. Side-by-side comparison between (a) reference geological map and (b) MLC classification for the Langkawi study area.

Table 9. NDVI-stratified map-derived agreement statistics.

NDVI class	Low	Moderate	Dense
NDVI range	0.024 – 0.478	0.478 – 0.712	0.712 – 0.993
Total pixels	22931	69567	370385
Correct pixels	13580	31176	194126
Map-derived agreement (%)	59.22%	44.81%	52.41%

F1-scores further confirmed the imbalance in class-level performance. Cm-SS/Sh/Md (65.22%), Qal (64.86%), and OS-Ls/SS (61.21%) showed relatively higher balanced performance, whereas PT-Ls/Mb (27.35%) and DP-St/Md (31.63%) showed weaker performance. These results indicate that carbonate-bearing and fine-grained sedimentary units were the most difficult to discriminate.

The JM separability matrix provides additional context for interpreting the confusion matrix. Although most training ROI pairs showed high statistical separability, relatively lower JM values were observed for OS-Ls/SS vs PT-Ls/Mb (1.807), DP-St/Md vs Tr-Gr (1.868), and DP-St/Md vs PT-Ls/Mb (1.892). These lower values are consistent with the stronger confusion among carbonate-bearing units, fine-grained sedimentary units, and weathered granitic terrain. However, high ROI-level separability did not necessarily translate into high island-scale agreement because the full-island classification included heterogeneous surfaces, transitional boundaries, vegetation cover, regolith, and mixed pixels.

To further examine the influence of vegetation cover, an NDVI-stratified map-derived agreement assessment was conducted. Water pixels were excluded, and the MLC classification was compared with the reference geological map within low-, moderate-, and dense-vegetation classes. The NDVI-stratified results (Table 9) show that map-derived agreement varied among vegetation-cover classes (Figure 9). Low-vegetation areas achieved the highest overall agreement (59.22%), followed by dense vegetation (52.41%) and moderate vegetation (44.81%). This non-linear pattern suggests that vegetation cover influenced lithological separability. However, the particularly low agreement in moderate-vegetation areas also reflects heterogeneous surfaces, including agriculture, settlement margins, exposed soil, regolith, and mixed pixels.

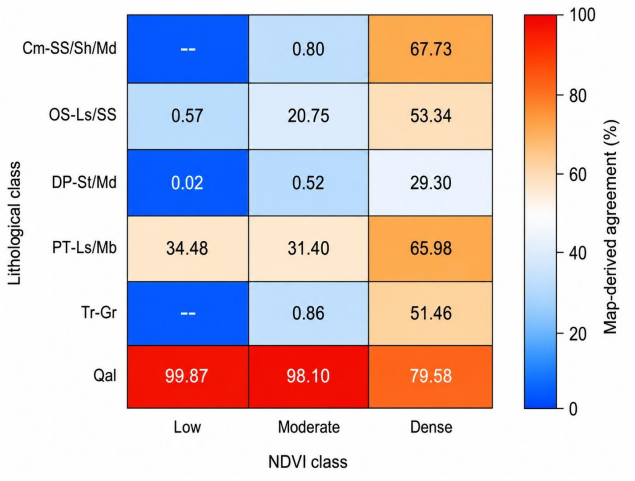

Figure 9. Heatmap of map-derived agreement (%) between lithological classes and NDVI-derived vegetation density classes.

The lithology-by-NDVI heatmap (Figure 9) further shows that vegetation-related effects were not uniform across lithological units. Qal maintained high agreement across all NDVI classes, whereas DP-St/Md showed consistently low agreement. Some carbonate-bearing and clastic units showed higher agreement in dense-vegetation areas than in moderate-vegetation areas, suggesting that dense-vegetation zones may coincide with more continuous lithological domains. In contrast, moderate-vegetation zones include more mixed and transitional surfaces.

6. DISCUSSION

6.1. Baseline Value of Landsat-9 OLI-2 Methods

The results confirm that classical Landsat-9 OLI-2 multispectral methods remain useful for first-order lithological interpretation across Langkawi Island. FCC, band ratios, OIF-guided band selection, and PCA enhanced broad contrasts among Alluvium, granitic terrain, and carbonate-bearing formations, while MLC reproduced part of the generalized geological framework. This supports previous findings that classical multispectral enhancement and classification methods can provide useful lithological information, but their value is mainly as a baseline or reconnaissance tool rather than as a definitive mapping approach [2], [8], [21], [24].

However, the moderate overall map-derived agreement of the MLC result and the uneven class-level performance indicate that Landsat-9 OLI-2 alone is insufficient for detailed unit-level discrimination in a densely vegetated tropical island environment. Therefore, the main value of the present workflow lies not in producing a definitive geological map, but in identifying which lithological units are broadly separable, which units remain confused, and where future multi-source or field-supported refinement is needed.

6.2. Island-scale Complexity Compared with Localized Langkawi Studies

Previous remote-sensing studies in the Langkawi archipelago mainly focused on localized areas. Simon et al. [2] identified useful band-ratio combinations for lithological discrimination in Dayang Bunting and Tuba Islands, while Du et al. [21] applied band-ratio techniques to lithological mapping in southern Langkawi. Compared with these local-scale studies, the full-island analysis conducted here spans a larger spatial extent, includes more diverse lithological assemblages, has more continuous vegetation cover, and involves more complex transitions among carbonate, clastic, granitic, and alluvial units. These conditions explain why the island-scale MLC result showed greater class confusion and only moderate map-derived agreement with the reference geological map.

This comparison suggests that results from localized areas should not be directly generalized to full-island mapping. At the local scale, fewer lithological classes, more restricted surface conditions, and smaller geological variability may allow band ratios and PCA to show clearer visual contrasts. At the island scale, however, the same methods are more strongly affected by mixed pixels, transitional boundaries, weathering, and vegetation cover. The contribution of this study is therefore to provide a full-island Landsat-9 baseline for Langkawi, against which future high-resolution, multi-source, or machine-learning-based mapping approaches can be evaluated.

6.3. Vegetation Influence on Lithological Separability

Vegetation cover was one of the main factors limiting lithological separability in this study. The NDVI analysis showed that Langkawi Island is dominated by dense vegetation, suggesting that many Landsat pixels likely contain mixed spectral contributions from vegetation, soil, weathered materials, and exposed rock rather than pure bedrock. As Chen et al. [25] emphasized, vegetation-covered regions are among the most challenging environments for lithological mapping because vegetation can obscure spectral information related to bedrock. This explains why lithological contrast in both image enhancement products and classification outputs was weakened in many parts of Langkawi, especially for units with similar surface expression or transitional boundaries.

The NDVI-stratified agreement assessment further supports this interpretation. Low-vegetation areas produced the highest map-derived agreement, suggesting stronger spectral contributions from exposed or weathered lithological surfaces, whereas moderate- and dense-vegetation areas showed lower agreement. However, the relationship between NDVI and map-derived agreement was not strictly linear: moderate-vegetation areas showed lower agreement than dense-vegetation areas, probably because they include more heterogeneous surfaces such as agricultural land, settlement margins, exposed soil, regolith, transition zones, and mixed pixels. Therefore, vegetation should not be interpreted as a single linear control on classification performance. Instead, lithological separability in Langkawi is likely influenced by multiple interacting factors, including vegetation cover, lithological distribution, terrain conditions, weathering intensity, mixed pixels, and uncertainty in reference map boundaries. This interpretation is supported by studies showing the value of DEM-derived variables [9], Sentinel-2/Sentinel-1/DEM fusion [16], and vegetation spectral features for improving lithological mapping in vegetated regions [57].

The higher agreement in dense-vegetation areas than in moderate-vegetation areas should not be interpreted as evidence that dense vegetation improves lithological discrimination. A more plausible explanation is that dense-vegetation zones are spatially associated

with more continuous upland lithological domains. In contrast, moderate-vegetation areas include more heterogeneous surfaces such as agriculture, settlement margins, exposed soil, regolith, and mixed vegetation. Consequently, moderate NDVI areas may contain stronger spectral mixing and more complex land-cover–lithology interactions, leading to lower map-derived agreement.

Although the NDVI-stratified agreement assessment helps reveal broad vegetation-related effects, it does not fully separate the influence of vegetation cover from lithological distribution, agricultural surfaces, settlement margins, exposed soil, regolith, and geological-map boundary uncertainty. A more detailed lithology-by-NDVI cross-analysis would further clarify how vegetation affects each lithological unit separately. However, because the present study aims to establish a Landsat-9 OLI-2 map-derived baseline rather than a full land-cover–lithology interaction model, this analysis is left for future work using field observations, higher-resolution imagery, and independent land-cover information.

6.4. Class Confusion and Lithological Interpretation

The MLC map-derived agreement results show clear differences among lithological units, indicating that class separability was influenced by spectral response, geomorphological setting, surface weathering, vegetation cover, and mixed pixels. Qal achieved the highest producer's agreement, suggesting that alluvial deposits were broadly detected because of their distinct lowland and coastal geomorphological setting. However, its moderate user's agreement indicates commission error, implying that some weathered regolith, exposed soil, and low-relief mixed surfaces were also classified as Alluvium. Similar uncertainty exists among surficial deposits, weathered materials, and exposed soil in Landsat- and ASTER-based lithological mapping studies [4], [22].

DP-St/Md was the most difficult unit to classify, with strong confusion, particularly with Qal and Tr-Gr. This is likely related to the subdued spectral response of dark fine-grained siltstone and mudstone, which can be further masked by tropical weathering, regolith development, soil cover, and vegetation. Chen et al. [25] similarly emphasized that vegetation, regolith, soil cover, mixed pixels, and limited bedrock exposure strongly constrain lithological mapping in vegetation-covered regions.

Carbonate-bearing units also showed classification uncertainty. The very low user agreement of PT-Ls/Mb suggests that the classifier over-assigned pixels to this class, while the confusion between OS-Ls/SS and PT-Ls/Mb may reflect spectral similarity among weathered limestone, carbonate-bearing surfaces, mixed carbonate–clastic materials, and vegetation-covered bedrock. Mohamed et al. [58] and Ghoneim et al. [17] also showed that conventional multispectral enhancement and classification methods can support broad lithological discrimination. However, class-level agreement may decline where lithological units have overlapping spectral responses. Therefore, the carbonate-related confusion observed in Langkawi helps define the practical boundary of classical Landsat-based mapping for separating spectrally similar formations under dense vegetation and tropical weathering conditions.

The difference between generally high JM separability and only moderate island-scale map-derived agreement is methodologically important. JM distance was calculated from selected training ROIs, intentionally chosen from relatively homogeneous areas and therefore representing the best-available spectral distinction among lithological classes. In contrast, the full-island classification includes heterogeneous vegetation cover, regolith, transitional lithological boundaries, coastal deposits, agricultural surfaces, settlement margins, and 30 m mixed pixels. Therefore, high ROI-level separability indicates that the training samples were statistically distinguishable, but it does not guarantee high agreement across the full island landscape.

In addition, the 30 m spatial resolution of Landsat-9 OLI-2 likely amplified mixed-pixel effects along lithological boundaries, narrow carbonate belts, coastal deposits, and heterogeneous agricultural or settlement margins. Some disagreement may also reflect differences between the generalized geological map boundaries and the spectral boundaries observable in satellite imagery. Therefore, part of the map-derived disagreement should be interpreted as a combined effect of sensor resolution, surface heterogeneity, transitional lithological boundaries, and reference-map uncertainty, rather than as classification error alone.

6.5. Implications, Limitations and Future Directions

The resulting lithological map should be interpreted as a reconnaissance-level, map-derived baseline rather than a substitute for detailed geological mapping. Its practical value lies in identifying broad lithological domains, highlighting areas of likely confusion, and indicating where future field checking or multi-source refinement is most needed. Persistent disagreement is particularly useful because it reveals where optical-only Landsat-9 OLI-2 is insufficient under dense vegetation, regolith cover, surface heterogeneity, and 30 m mixed-pixel conditions.

This baseline also provides a diagnostic reference for designing future multi-source lithological mapping strategies. Sentinel-1 SAR may add structural and surface-roughness information, DEM-derived variables may improve terrain-controlled lithological interpretation, and Sentinel-2 or ASTER data may improve spectral separability. Future studies should combine these data sources with field observations and advanced classifiers to test whether the limitations identified in this study can be reduced.

7. CONCLUSION

This study evaluated the applicability and limitations of Landsat-9 OLI-2 and classical multispectral techniques for island-scale lithological discrimination in Langkawi Island. FCC, OIF-based band selection, band-ratio analysis, and PCA enhanced broad lithological contrasts among Alluvium, granitic terrain, and carbonate-bearing formations. The MLC classification achieved an overall map-derived agreement of 51.72% and a kappa coefficient of 0.4177 when compared with the published geological map, indicating moderate agreement with the existing geological framework.

The findings show that detailed lithological discrimination remains limited in densely vegetated humid tropical island environments. Qal was more readily detected, whereas DP-St/Md, Tr-Gr, and carbonate-bearing units showed stronger confusion. The NDVI-stratified and lithology-by-NDVI results further indicate that vegetation effects were not uniform across lithological units and that moderate-vegetation zones may contain especially heterogeneous surfaces. These limitations are associated with vegetation cover, tropical weathering, regolith and soil cover, mixed pixels, lithological similarity, reference-map uncertainty, and the 30 m spatial resolution of Landsat-9 OLI-2.

The study provides a full-island, map-derived baseline rather than an independently field-validated lithological map. Future work should integrate Sentinel-1 SAR, DEM-derived variables, Sentinel-2 or ASTER data, field observations, and advanced classifiers to improve lithological discrimination in humid tropical island settings.

ACKNOWLEDGMENTS

The authors would like to thank the Geophysics Program, School of Physics, Universiti Sains Malaysia (USM), for its academic support during this study. We are also grateful to the U.S. Geological Survey (USGS) for providing the Landsat-9 OLI-2 data used in this research. The authors further thank the reviewers for their valuable comments and suggestions.

CONFLICTS OF INTEREST

The authors declare that no conflicts of interest are associated with this study. All aspects of the research were conducted with the utmost integrity and transparency.

DATA AVAILABILITY

The datasets utilized and analyzed during this research are available from the corresponding author upon reasonable request.

ETHICAL STATEMENTS

Not applicable. This study did not involve any human participants or animals, and no personal or sensitive data were collected, used, or analyzed at any stage of the research.

FUNDING

This research was conducted without financial support. The authors confirm that no funding was received for this study's research, analysis, or publication.

REFERENCES

[1] J. M. Akhir and I. Abdullah, “Geological applications of LANDSAT thematic mapper imagery: mapping and analysis of lineaments in NW Peninsula Malaysia,” UNI. Kebangssan, Malaysia. AARS Pap. ACRS1997, Geol., 1997, [Online]. Available: https://acrs-aars.org/proceeding/ACRS1997/Papers/GEO97-1.htm

[2] N. Simon, C. Aziz Ali, K. R. Mohamed, and K. Sharir, “Best band ratio combinations for the lithological discrimination of the Dayang Bunting and Tuba Islands, Langkawi, Malaysia,” Sains Malaysiana, vol. 45, no. 5, pp. 659–667, 2016, [Online]. Available: http://journalarticle.ukm.my/9868/

[3] A. Joseph and O. Bamidele, “Application of remote sensing method for geological interpretation of Sokoto Plain, Nigeria,” South African J. Geomatics, vol. 7, no. 3, p. 360, 2019, https://doi.org/10.4314/sajg.v7i3.12

[4] S. A. Aliyan, A. S. Bratanegara, H. M. Ihsan, A. J. Astari, and L. Somantri, “Identification of Lithological Characteristics Using Multispectral Landsat 8 OLI Imagery in the Cipatujah Area, West Java, Indonesia,” in IOP Conference Series: Earth and Environmental Science, 2022, vol. 1089, no. 1, p. 12021. https://doi.org/10.1088/1755-1315/1089/1/012021

[5] L. Yan and D. P. Roy, “Using Landsat 8 and 9 operational land imager (OLI) data to characterize geometric distortion and improve geometric correction of Landsat Multispectral Scanner (MSS) imagery,” Remote Sens. Environ., vol. 321, p. 114679, 2025, https://doi.org/10.1016/j.rse.2025.114679

[6] A. B. Pour, M. Hashim, J. K. Hong, and Y. Park, “Lithological and alteration mineral mapping in poorly exposed lithologies using Landsat-8 and ASTER satellite data: North-eastern Graham Land, Antarctic Peninsula,” Ore Geol. Rev., vol. 108, pp. 112–133, 2019, https://doi.org/10.1016/j.oregeorev.2017.07.018

[7] C. Kumar, A. Shetty, S. Raval, R. Sharma, and P. K. C. Ray, “Lithological discrimination and mapping using ASTER SWIR Data in the Udaipur area of Rajasthan, India,” Procedia Earth Planet. Sci., vol. 11, pp. 180–188, 2015, https://doi.org/10.1016/j.proeps.2015.06.022

[8] R. Mohamed, J. Tamen, S. Ousmanou, F. K. Yangouo, and D. Nkouathio, “Lithological discrimination based on Landsat-9 OLI sensor and field observation data: The bana an-orogenic volcano-plutonic ring complex, West Cameroon line,” Heliyon, vol. 10, no. 17, 2024, https://doi.org/10.1016/j.heliyon.2024.e36806

[9] Y. Chen, Y. Dong, Y. Wang, F. Zhang, G. Liu, and P. Sun, “Machine learning algorithms for lithological mapping using Sentinel-2 and SRTM DEM in highly vegetated areas,” Front. Ecol. Evol., vol. 11, p. 1250971, 2023. https://doi.org/10.3389/fevo.2023.125097

[10] H. Ghrefat, A. Y. Kahal, K. Abdelrahman, H. J. Alfaifi, and S. Qaysi, “Utilization of multispectral landsat-8 remote sensing data for lithological mapping of southwestern Saudi Arabia,” J. King Saud Univ. - Sci., vol. 33, no. 4, p. 101414, 2021, https://doi.org/10.1016/j.jksus.2021.101414

[11] Z. Ourhzif, A. Algouti, A. Algouti, and F. Hadach, “Lithological mapping using landsat 8 oli and aster multispectral data in imini-ounilla district south high atlas of marrakech,” Int. Arch. Photogramm. Remote Sens. Spat.

Inf. Sci. - ISPRS Arch., vol. 42, no. 2/W13, pp. 1255–1262, 2019, https://doi.org/10.5194/isprs-archives-XLII-2-W13-1255-2019

[12] A. Shebl and M. Hamdy, "Multiscale (microscopic to remote sensing) preliminary exploration of auriferous-uraniferous marbles: A case study from the Egyptian Nubian Shield," Sci. Rep., vol. 13, no. 1, p. 9173, 2023, https://doi.org/10.1038/s41598-023-36388-7

[13] M. A. EL-Omairi and A. El Garouani, "A review on advancements in lithological mapping utilizing machine learning algorithms and remote sensing data," Heliyon, vol. 9, no. 9, 2023, https://doi.org/10.1016/j.heliyon.2023.e20168

[14] A. Shebl et al., "Impact of DEMs for Improvement Sentinel 2 Lithological Mapping Utilizing Support Vector Machine: A Case Study of Mineralized Fe-Ti-Rich Gabbroic Rocks from the South Eastern Desert of Egypt," Minerals, vol. 13, no. 6, p. 826, 2023, https://doi.org/10.3390/min13060826

[15] H. Bahrami, P. Esmaeili, S. Homayouni, A. B. Pour, K. Chokmani, and A. Bahroudi, "Machine Learning-Based Lithological Mapping from ASTER Remote-Sensing Imagery," Minerals, vol. 14, no. 2, p. 202, 2024, https://doi.org/10.3390/min14020202

[16] Y. Chen, G. Liu, Z. Song, M. Li, M. Wang, and S. Wang, "Lithological Mapping in High-Vegetation Areas Using Sentinel-2, Sentinel-1, and Digital Elevation Models," Sensors, vol. 25, no. 7, p. 2136, 2025, https://doi.org/10.3390/s25072136

[17] S. M. Ghoneim, Z. Hamimi, K. Abdelrahman, M. A. Khalifa, M. Shabban, and A. S. Abdelmaksoud, "Machine learning and remote sensing-based lithological mapping of the Duwi Shear-Belt area, Central Eastern Desert, Egypt," Sci. Rep., vol. 14, no. 1, p. 17010, 2024, https://doi.org/10.1038/s41598-024-66199-3

[18] T. Zhang et al., "Rapid lithological mapping using multi-source remote sensing data fusion and automatic sample generation strategy," Int. J. Digit. Earth, vol. 17, no. 1, p. 2420824, 2024, https://doi.org/10.1080/17538947.2024.2420824

[19] F. F. Sabins, "Remote sensing for mineral exploration," Ore Geol. Rev., vol. 14, no. 3–4, pp. 157–183, 1999, https://doi.org/10.1016/S0169-1368(99)00007-4

[20] P. S. Chavez, G. L. Berlin, and L. B. Sowers, "Statistical Method for Selecting Landsat Mss Ratios.," J. Appl. Photogr. Eng., vol. 8, no. 1, pp. 23–30, 1982.

[21] Y. Du, Y. J. Teoh, I. A. Abir, R. P. Jaya, and Y. Ulfa, "Lithological distribution using band ratio technique in Southern Langkawi, Kedah, Malaysia," Environ. Sci. Pollut. Res., pp. 1–13, 2025, https://doi.org/10.1007/s11356-025-36465-6

[22] A. Marzouki and A. Dridri, "Lithological discrimination and structural lineaments extraction using Landsat 8 and ASTER data: a case study of Tiwit (Anti-Atlas, Morocco)," Environ. Earth Sci., vol. 82, no. 5, p. 125, 2023, https://doi.org/10.1007/s12665-023-10831-4

[23] M. Dawoud et al., "Applications of Remote Sensing in Lithological Mapping of East Gabal Atud Area, Central Eastern Desert, Egypt," Geo-Eco-Marina, vol. 29, pp. 125–146, 2023, [Online]. Available: https://journal.geoecomar.ro/geo-eco-marina/article/view/11_2023

[24] S. Ali, H. Li, A. Ali, and J. I. Hassan, "Lithological Discrimination of Khyber Range Using Remote Sensing and Machine Learning Algorithms," Appl. Sci., vol. 14, no. 12, p. 5064, 2024, https://doi.org/10.3390/app14125064

[25] Y. Chen, Y. Wang, F. Zhang, Y. Dong, Z. Song, and G. Liu, "Remote Sensing for Lithology Mapping in Vegetation-Covered Regions: Methods, Challenges, and Opportunities," Minerals, vol. 13, no. 9, p. 1153, 2023, https://doi.org/10.3390/min13091153

[26] A. Shebl, M. Abdellatif, M. Hissen, M. Ibrahim Abdelaziz, and Á. Csámer, "Lithological mapping enhancement by integrating Sentinel 2 and gamma-ray data utilizing support vector machine: A case study from Egypt," Int. J. Appl. Earth Obs. Geoinf., vol. 105, p. 102619, 2021, https://doi.org/10.1016/j.jag.2021.102619

[27] J. Xi, Q. Jiang, H. Liu, and X. Gao, "Lithological Mapping Research Based on Feature Selection Model of ReliefF-RF," Appl. Sci., vol. 13, no. 20, p. 11225, 2023, https://doi.org/10.3390/app132011225

[28] Z. Wang and R. Zuo, "Intelligent Lithological Mapping: Challenges and Future Prospective," Nat. Resour. Res., pp. 1–34, 2025, https://doi.org/10.1007/s11053-025-10563-1

[29] C. R. Jones, "Geology and mineral resources of Perlis, north Kedah and the Langkawi Ialands.," Geol. Surv. Malaysia, vol. 17, p. 257, 1978, [Online]. Available: https://elib.jmg.gov.my/cgi-bin/koha/opac-detail.pl?biblionumber=33

[30] C. P. Lee, "Review of the Palaeozoic Stratigraphy of the Langkawi Islands, Malaysia," Indones. Sedimentol. Forum Sedimentol. Comm. - Indones. Assoc. Geol., vol. 8, no. 27, pp. 5–14, 2013, https://doi.org/10.51835/bsed.2013.27.1.157

[31] L. R. M. Cocks, R. A. Fortey, and C. P. Lee, "A review of Lower and Middle Palaeozoic biostratigraphy in west peninsular Malaysia and southern Thailand in its context within the Sibumasu Terrane," J. Asian Earth Sci., vol. 24, no. 6 SPEC. ISS., pp. 703–717, 2005, https://doi.org/10.1016/j.jseaes.2004.05.001

[32] W. F. Wan Hassan, "On some ore and skarn minerals of Langkawi," Bull. Geol. Soc. Malaysia, vol. 46, pp. 217–221, 2003, https://doi.org/10.7186/bgsm46200336

[33] K. R. Mohamed, T. Unjah, C. A. Ali, and M. H. Kamal Roslan, "Geosite mapping of pulau ular in langkawi, Malaysia," Sains Malaysiana, vol. 48, no. 11, pp. 2511–2519, 2019, https://doi.org/10.17576/jsm-2019-4811-21

[34] I. Metcalfe, "The Bentong–Raub Suture Zone," J. Asian Earth Sci., vol. 18, no. 6, pp. 691–712, 2000, https://doi.org/10.1016/S1367-9120(00)00043-2

[35] T. Unjah and S. A. Halim, "Connecting legend and science through geomythology: Case of Langkawi unesco global geopark," Kaji. Malaysia, vol. 35, pp. 77–89, 2017, https://doi.org/10.21315/KM2017.35.SUPP.1.5

[36] L. C. Rowan and J. C. Mars, "Lithologic mapping in the Mountain Pass, California area using Advanced Spaceborne Thermal Emission and Reflection Radiometer (ASTER) data," Remote Sens. Environ., vol. 84, no. 3, pp. 350–366, 2003, https://doi.org/10.1016/S0034-4257(02)00127-X

[37] F. D. van der Meer et al., "Multi- and hyperspectral geologic remote sensing: A review," Int. J. Appl. Earth Obs. Geoinf., vol. 14, no. 1, pp. 112–128, 2012, https://doi.org/10.1016/j.jag.2011.08.002

[38] Y. Ninomiya, B. Fu, and T. J. Cudahy, "Detecting lithology with Advanced Spaceborne Thermal Emission and Reflection Radiometer (ASTER) multispectral thermal

infrared 'radiance-at-sensor' data," Remote Sens. Environ., vol. 99, no. 1–2, pp. 127–139, 2005, https://doi.org/10.1016/j.rse.2005.06.009

[39] A. B. Pour and M. Hashim, "Hydrothermal alteration mapping from Landsat-8 data, Sar Cheshmeh copper mining district, south-eastern Islamic Republic of Iran," J. Taibah Univ. Sci., vol. 9, no. 2, pp. 155–166, 2015, https://doi.org/10.1016/j.jtusci.2014.11.008

[40] M. Sekandari et al., "Application of Landsat-8, Sentinel-2, ASTER and Worldview-3 spectral imagery for exploration of carbonate-hosted Pb-Zn deposits in the Central Iranian Terrane (CIT)," Remote Sens., vol. 12, no. 8, p. 1239, 2020, https://doi.org/10.3390/RS12081239

[41] G. Chander, B. L. Markham, and D. L. Helder, "Summary of current radiometric calibration coefficients for Landsat MSS, TM, ETM+, and EO-1 ALI sensors," Remote Sens. Environ., vol. 113, no. 5, pp. 893–903, 2009, https://doi.org/10.1016/j.rse.2009.01.007

[42] K. W. Abdelmalik, "Landsat 8: Utilizing sensitive response bands concept for image processing and mapping of basalts," Egypt. J. Remote Sens. Sp. Sci., vol. 23, no. 3, pp. 263–274, 2020, https://doi.org/10.1016/j.ejrs.2019.04.004

[43] C. J. Tucker, "Red and photographic infrared linear combinations for monitoring vegetation," Remote Sens. Environ., vol. 8, no. 2, pp. 127–150, 1979, https://doi.org/10.1016/0034-4257(79)90013-0

[44] S. A. Drury, "Image interpretation in geology," Geocarto Int., vol. 2, no. 2, p. 48, 1987, https://doi.org/10.1080/10106048709354098

[45] E. A. Ali, "Landsat ETM+7 Digital Image Processing Techniques for Lithological and Structural Lineament Enhancement: Case Study Around Abidiya Area, Sudan," Open Remote Sens. J., vol. 5, no. 1, pp. 83–89, 2012, https://doi.org/10.2174/1875413901205010083

[46] A. Julzarika, N. Anggraini, and S. W. Adawiah, "Detection of True Mangroves in Indonesia Using Satellite Remote Sensing," J. Environ. Anal. Prog., pp. 157–167, 2019, https://doi.org/10.24221/jeap.4.3.2019.2488.157-167

[47] F. Masoumi, T. Eslamkish, A. A. Abkar, M. Honarmand, and J. R. Harris, "Integration of spectral, thermal, and textural features of ASTER data using Random Forests classification for lithological mapping," J. African Earth Sci., vol. 129, pp. 445–457, 2017, https://doi.org/10.1016/j.jafrearsci.2017.01.028

[48] Z. Adiri, A. El Harti, A. Jellouli, L. Maacha, and E. M. Bachaoui, "Lithological mapping using multispectral ASTER and Landsat 8 data in the Bas Drâa inlier, Moroccan Anti Atlas," Earth Resour. Environ. Remote Sensing/GIS Appl. VI, vol. 9644, no. 1, p. 96440L, 2015, https://doi.org/10.1117/12.2193775

[49] B. Munkhsuren, B. Enkhdalai, T. Narantsetseg, K. Udaanjargal, D. Orolmaa, and D. Munkhjin, "Lithological mapping using remote sensing techniques: A case study of Alagbayan area, Dornogobi province, Mongolia," Mong. Geosci., vol. 26, no. 53, pp. 37–54, 2021, https://doi.org/10.5564/mgs.v26i53.1790

[50] T. M. Lillesand and R. W. Kiefer, Remote sensing and image interpretation. John Wiley & Sons, 1979. https://doi.org/10.2307/634969

[51] J. A. Richards, Remote sensing digital image analysis: An introduction, vol. 9783642300. Springer, 2013. https://doi.org/10.1007/978-3-642-30062-2

[52] I. Bentahar and M. Raji, "Comparison of Landsat OLI, ASTER, and Sentinel 2A data in lithological mapping: A Case study of Rich area (Central High Atlas, Morocco)," Adv. Sp. Res., vol. 67, no. 3, pp. 945–963, 2021, https://doi.org/10.1016/j.asr.2020.10.037

[53] R. G. Congalton and K. Green, Assessing the accuracy of remotely sensed data: Principles and practices, second edition. CRC press, 2008.

[54] K. Kulkarni and P. A. Vijaya, "Separability analysis of the band combinations for land cover classification of satellite images," Int. J. Eng. Trends Technol., vol. 69, no. 8, pp. 138–144, 2021, https://doi.org/10.14445/22315381/IJETT-V69I8P217

[55] A. Laake, "Integration of Satellite Imagery, Geology and Geophysical Data," Earth Environ. Sci., pp. 467–492, 2011, https://doi.org/10.5772/27613

[56] M. K. Tripathi, H. Govil, and P. Diwan, "Lithological mapping using digital image processing techniques on landsat 8 OLI remote sensing data in Jahajpur, Bhilwara, Rajasthan," in 2019 2nd International Conference on Intelligent Communication and Computational Techniques, ICCT 2019, 2019, pp. 43–48. https://doi.org/10.1109/ICCT46177.2019.8969043

[57] Y. Lu, C. Yang, and L. Han, "Mapping bedrock with vegetation spectral features using time series Sentinel-2 images," Geocarto Int., vol. 38, no. 1, p. 2236574, 2023, https://doi.org/10.1080/10106049.2023.2236574

[58] M. A. El-Omairi and A. El Garouani, "Lithological Mapping using Artificial Intelligence and Remote Sensing data: A Case Study of Bab Boudir region, Morocco," in BIO Web of Conferences, 2024, vol. 115, p. 1005. https://doi.org/10.1051/bioconf/202411501005